A New Hardness Formula Incorporating the Effect of Source Density on Indentation Response: A Discrete Dislocation Plasticity Analysis

Y. Xu, D.S. Balint, D. Dini[1]

[1]Department of Mechanical Engineering, Imperial College London, London SW7 2AZ, UK

Abstract

Planar discrete dislocation plasticity (DDP) calculations that simulate thin single crystal films bonded to a rigid substrate indented by a rigid wedge are performed for different values of film thickness and dislocation source density. As in prior studies, an indentation size effect (ISE) is observed when indentation depth is sufficiently small relative to the film thickness. The dependence of the ISE on dislocation source density is quantified in this study, and a modified form of the scaling law for the dependence of hardness on indentation depth, first derived by Nix and Gao, is proposed, which is valid over the entire range of indentation depths and correlates the length scale parameter with the average dislocation source spacing. Nano-indentation experimental data from the literature are fitted using this formula, which further verifies the proposed scaling of indentation pressure on dislocation source density.

Keywords: Discrete dislocation plasticity; Indentation; Hardness; Thin Films; Single Crystals.

[1] Corresponding author: d.dini@imperial.ac.uk ; Tel./Fax: +44 (0) 207 594 7242.

1 Introduction

Small-scale indentation is increasingly used to measure yield stress and Young's modulus for thin films and small material volumes. It has been established experimentally that continuum relationships for hardness applicable to large scale conical (or pyramidal) and spherical indentation [1, 2] fail when indentation depths are sufficiently small (nano/micro); the observation is that which is typical of nearly all material size effects, *i.e.* that sufficiently small indentation depths correspond to larger indentation pressures [3-9].

Among the early models of the indentation size effect (ISE), Nix and Gao [10] developed an analytical formula that predicts size-dependent hardness based on geometrically necessary dislocations and the strain gradient. Some further work based on strain gradients was conducted in Refs. [11-14], in order to study the relationship between the indentation size effect and material length scale parameters. Taylor-based nonlocal theory (TNT) of plasticity was developed in [15], a strain gradient form of non-local plasticity theory [16], which is capable of capturing the ISE.

Continuum methods require fitting a length scale parameter to experimental data, *e.g.* the formula developed by Nix and Gao worked reasonably well to capture the experimental behaviour [17] after suitably fitting a length scale parameter in the model to the data. On the other hand, the length scales in discrete dislocation plasticity, which capture dislocation mediated size effects naturally, are measurable and have clear origins in the microstructure. The indentation size effect has been studied in detail using discrete dislocation plasticity methods. Among them, the work of Balint et al. [18] found that the formula of Nix and Gao was capable of fitting *nominal* indentation pressure versus depth reasonably well. However, it was found that the material length scale parameter assumed a physically reasonable value on the order of the source spacing only when the scaling exponent n of the relationship was allowed to deviate from the usual 0.5, to 0.65-0.7. Furthermore, the form of the Nix and Gao formula was not able to fit the prediction for *actual* indentation pressure versus depth. In addition, the effect of source density on the material hardness was qualitatively investigated in [18, 19], but a scaling relationship was not identified.

The dislocation source density parameter provides a natural link between the material response and the average source spacing. Source limited behaviour has been observed in prior DDP studies of tension [20, 21] and cantilever beam bending [22, 23]. Although the effect of source density on hardness was discussed briefly in [24], a quantitative study and scaling relationship between hardness and source density has not been identified.

While the Nix and Gao model [10] and its variants, *e.g.* [25, 26], are based on geometrically necessary dislocations (GNDs) to give the indentation size effect at the micrometre length scale at room temperature, suggestions have been made by others that GNDs are not observed during the early stages of indentation [27], hence that the ISE may be controlled by other mechanisms, such as thermal activation. Franke et al. [28] experimentally observed that an elevated temperature reduced the ISE in copper; a similar trend was observed at lower temperatures in [29], depending on the propensity of the material to cross slip. Maughan et al. [30] found that various factors, including dislocation density, grain size, etc., play a significant role in the ISE.

In this paper, we propose a new indentation pressure formula based on the Nix and Gao model that captures the finite, zero indentation depth elastic hardness limit, in addition to the size effect region and the depth-independent continuum limit, which also provides an

interpretation and quantitative link between the length scale parameter in the formula and the average dislocation source spacing.

The article is organised as follows: Section 2 provides a summary of the planar discrete dislocation plasticity method used by the authors and defines the problem under investigation, including key parameters used in this study. Section 3 provides the derivation of the new formula based on the original Nix and Gao approach [10]; this is followed by physical interpretation of each individual parameter identified, and the provision of guidelines for their derivation via modelling and/or experimental investigation; this section concludes with the fitting of a wide range of experimental data for validation purposes. Section 4 provides an in-depth discussion of the findings shown in Section 3, and Section 5 summarises the key findings with concluding remarks.

2 Numerical Methodology

2.1 Discrete dislocation plasticity (DDP) formulation

In this study, we use a model based on the planar discrete dislocation plasticity (DDP) computational framework established by Van der Giessen and Needleman [3]. This framework has been extensively applied to study fundamental problems at the micro-scale, including size effects in uniaxial tension (*e.g.* [31]), compression of micro-pillars (*e.g.* [32]), micro-indentation (*e.g.* [33, 34]), bending ([22, 23]), etc. In particular, we focus on the nano-indentation problem studied by Xu et al. [35], with the aim of capturing the source density dependence of the ISE, and to derive a scaling relationship for hardness that captures the ISE and is valid for all indentation depths.

The thin film is modelled as a FCC single crystal, and the 2D plane of interest is taken perpendicular to the $[10\bar{1}]$ crystallographic direction to satisfy the plane strain constraint (please refer to Ref. [20] and [36] for discussion of this configuration), *i.e.* $\varepsilon_{33} = \varepsilon_{13} = \varepsilon_{23} = 0$.

Extensive details of the planar DD formulation can be found in [3]; key points of the methodology are given here, with parameter choices specified in Section 2.2. The loading is applied incrementally (see Section 2.2) and the dislocation structure is evolved quasi-statically. At every time-step of the simulation, the displacement, strain and stress fields are obtained from the linear superposition of two fields (see eq.(1)), respectively, as defined in [3]. The $\widetilde{(\ )}$ fields arise from the cumulative contribution of the infinite body fields of the dislocations within the specimen, while the $\widehat{(\ )}$ fields are the correction needed to satisfy the applied tractions and displacements on the finite boundary. The linear superposition scheme is illustrated schematically in Figure 1.

$$\begin{aligned} \boldsymbol{u} &= \widetilde{\boldsymbol{u}} + \widehat{\boldsymbol{u}} \\ \boldsymbol{\sigma} &= \widetilde{\boldsymbol{\sigma}} + \widehat{\boldsymbol{\sigma}} \\ \boldsymbol{\varepsilon} &= \widetilde{\boldsymbol{\varepsilon}} + \widehat{\boldsymbol{\varepsilon}} \end{aligned} \tag{1}$$

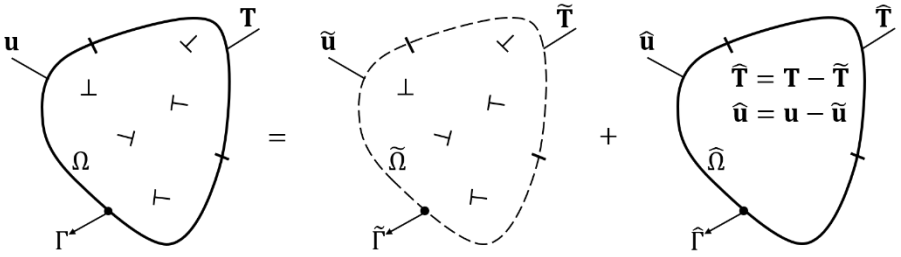

Figure 1. The superposition scheme of the planar DDP formulation.

The specimen is initially assumed to be dislocation free but is populated with a specified density of dislocation nucleation sites and obstacles. A dipole of dislocations, representing a planar cut of a dislocation loop through its pure edge segments, is nucleated if the predefined threshold shear stress τ_{nuc} is reached at a nucleation site and maintained for the nucleation period t_{nuc}. Temperature can affect dislocation nucleation and motion by its influence on the nucleation strength and drag coefficient, as well as the elastic properties [37, 38], however the nano-indentation process studied here is assumed to be isothermal ($\mathrm{T} = 20°\mathrm{C}$), representative of the quasi-static indentation processes commonly used to measure strain rate independent material properties; significant temperature change is not expected to occur in this situation, hence the influence of temperature is ignored in our simulations.

The nucleation time is taken to be a constant $t_{nuc} = 10ns$, as estimated in Ref. [39], in all simulations; this is sufficiently large for the nucleated loop to achieve its unstable configuration as stated in Ref. [39]. The only factors that can affect rate sensitivity in the model are the nucleation time and the drag coefficient, *i.e.* additional sources of rate sensitivity such as escape of dislocations from obstacles, as discussed for example in Ref. [40], are excluded from this investigation. New dislocation dipoles are spaced apart by $L_{nuc} = \frac{Gb}{2\pi\tau_{nuc}(1-\nu)}$, and sources are distributed randomly on the slip planes with nucleation strengths taken from a Gaussian distribution (representing the population of trapped dislocation line lengths in the material) with the parameters given in Table 1; hence a distribution of dipole spacings results from the distribution of source strengths. Although the nucleation dipole distance can evolve with the dislocation density [41], that effect is not expected to be significant in the present work. This assumption has been widely used in other indentation calculations using the DDP framework, *e.g.* [18, 42].

Once nucleated, dislocations are assigned a glide velocity (there is no dislocation climb in the simulations) from a linear mobility law [43], based on the Peach-Koehler force acting on the dislocation and a specified drag coefficient, B. A cut-off velocity of $20\ m/s$ was used to prevent the need for extremely small time increments without sacrificing the micro-mechanistic features. The effect of introducing a cut off velocity was discussed in *e.g.* Ref. [44]. Finite deformations effects, as studied in Ref. [45], are neglected in this study; a small strain assumption has been made. Other DDP associated parameters are the same as those set in the study presented in Ref. [35]. Further details of the formulation can be found in [3].

2.2 Problem definition

Starting from the investigation reported in Ref. [35], whose focus was to utilize a multi-scale coupling method to study the response of a thin film across the scales, we now perform simulations to shed light on the indentation pressure response of the thin film, *i.e.* the coating material, for very small values of indentation depth and as a function of the dislocation source density. We therefore aim to explore the effect that material defects and dislocation structures have on the material response. A DDP description of the wedge indentation of a

single crystal aluminium-like film characterized by dimension $h \times l$ bonded by a rigid substrate was analysed, see Figure 2, where l is the length of the dislocation process window, which is fixed as $l = 30\,\mu m$ for a film of length $L = 1000\,\mu m$. The region outside the dislocation activity region is modelled as elastic. Here the thickness of the thin film is varied as $h = 10, 20, 30, 50 \text{ and } 100 \mu m$. Plasticity in the DDP process window is the result of the collective motion of edge type dislocations along predefined slip planes.

The indenter is modelled as a rigid wedge, whose surface is inclined by an angle $\alpha = 5°$ with respect to the *x* axis. The indenter shape is the same as in the research presented in Ref. [35], where the contact condition was discussed in more detail. There are three predefined slip systems in the thin film oriented by $\phi^s = \pm 35.3, 90, s = 1, 2, 3$ with respect to the *y*-axis. We vary the density of nucleation sources and obstacles in a wide range, which aims to reveal the source spacing effect on the indentation pressure of the films. Other computational parameters are summarized in Table 1.

Table 1. DDP material parameters used in the wedge-shaped indentation problem.

Parameter Name	Symbol	Unit	Value
Young's Modules	E	GPa	70
Poisson Ratio	υ	-	0.33
Burger's Vector	b	nm	0.25
Spacing of Slip Planes	-	nm	100b
Drag Coefficient	B	$\text{Pa} \cdot \text{s}$	10^{-4}
Annihilation Distance	L_e	nm	6b
Source Strength Mean	$\bar{\tau}_{\text{nuc}}$	MPa	50
Source Strength standard deviation	–	MPa	10
Obstacle Strength	τ_{obs}	MPa	150
Nucleation Time	t_{nuc}	ns	10

The computation of an indentation history is carried out in an incremental manner with a monotonically increasing value of applied indentation depth with a constant rate prescribed as $\dot{\delta}$. Perfect sticking boundary conditions are imposed along the contact boundary between the process window upper surface and the indenter. Thus, the boundary conditions are:

$$\dot{u}_x = 0, \dot{u}_y = \dot{\delta} \quad \text{on} \quad S_{\text{contact}} \tag{2}$$

In eq. (2) , S_{contact} represents the fraction of the upper surface in contact with the indenter and δ is the indentation depth. The nominal contact size, $A_N \equiv 2d/\tan(\alpha)$, and actual contact size A, which is defined as the distance between the rightmost and leftmost nodes within the contact, were used, as in Ref. [46]. The nominal and actual contact sizes are in general different, and the difference depends on the degree of pile-up or sink-in experienced during indentation. This is discussed in detail in Refs. [18, 19, 35], where the correlation between surface behaviour during indentation and contact size is revealed. The definition of A and A_N is sketched in Figure 3(b). In this study we ignore the contribution of surface roughness, which can also be incorporated as shown in Ref. [47].

The fixed boundary conditions and free surface conditions are imposed as:

$$\dot{u}_y = 0 \quad \text{on} \quad y = 0 \quad \text{with} \quad \dot{u}_x = 0 \quad \text{at} \quad x = 0 \tag{3}$$

$$T_x = T_y = 0 \quad \text{on} \quad x = h \notin S_{contact}. \tag{4}$$

In eq. (4), $T_i = \sigma_{ij} n_j$ is the surface traction on a surface with its outward normal vector n_j. The total normal reaction force of the thin film in response to the indenter penetration is computed as the integral of the traction along the contact:

$$F = -\int_{-A/2}^{A/2} T_2(x,h)dx \tag{5}$$

According to the definition of nominal and actual contact size, the actual and nominal indentation pressure, p_A and p_N, are correspondingly computed as the ratio of the total normal reaction force to the actual and nominal contact length, respectively, which gives:

$$p_A = F/A \tag{6}$$

$$H \equiv p_{\mathrm{N}} = F/A_N \tag{7}$$

In this research, we mainly consider the definition of nominal indentation pressure, p_{N}, to represent the hardness of a material as the jumps in the actual indentation pressure, p_A, introduce difficulties in numerical fitting.

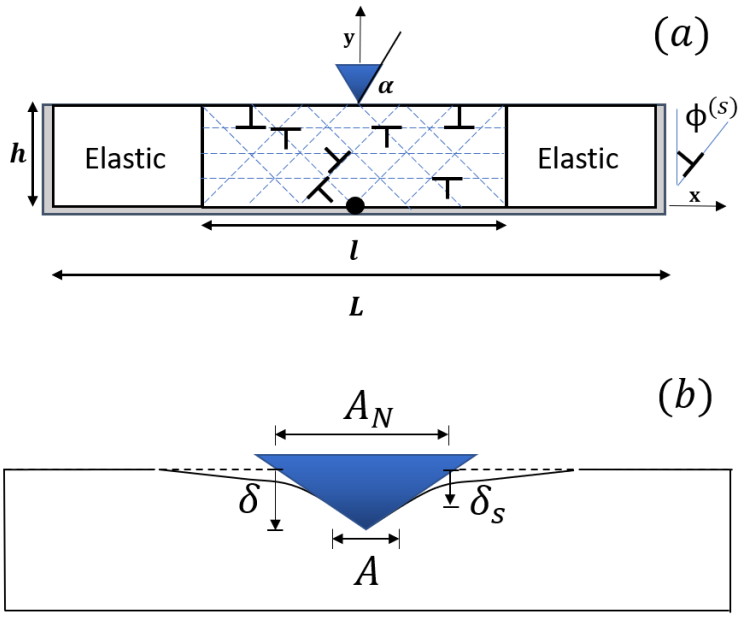

Figure 2. (a) Sketch of the indentation boundary value problem solved using the DDP computational framework. The black circle denotes the coordinate system origin. (b) The definitions of the actual contact size A, the nominal contact area A_N, the indentation depth δ and the sink-in depth δ_s. The calculations ignored the surface roughness.

Based on the definitions from eq. (6) and (7), the indentation pressure requires determining the contact size, which depends on the mesh size used along the contact edge. Therefore, we applied a highly biased mesh (the biased ratio is up to 60) from the contact middle point to the edge of the process window. The finest mesh is allocated near the indenter tip in order to obtain a higher spatial resolution within the contact and, thus, to accurately capture the gradients of the field parameters in the DDP region. This highly focused mesh improves the accuracy of the indentation response, particularly when the indentation depth is extremely small. The mesh convergence analysis performed as part of this study showed that further refinement did not improve the accuracy, even when the indentation depth was very small. Please see Section 3.3 for further discussion.

A rate of indentation displacement $\dot{\delta} = 0.4\ \mathrm{m} \cdot \mathrm{s}^{-1}$ was imposed on the rigid indenter in order to improve the computational efficiency. This rate was found to reasonably capture the

quasi-static indentation pressure response [18], although the detailed dislocation structure within the thin film can vary under different loading rates, as shown in DDP calculations performed by other researchers, see *e.g.* [48, 49]. The time step $\Delta t = 0.5ns \ll t_{nuc}$ is used in all simulations. All the indentation simulations shown in this paper achieved an applied indentation depth of $\delta = 300\,\mathrm{nm}$, where the indentation pressure response normally reaches the indentation depth independent limit, *i.e.* the macroscopic continuum hardness value.

3 Results and Discussion

3.1 Indentation size effect captured via DDP

Actual indentation pressure p_A curves versus applied indentation depth δ are plotted in Figure 3(a) for three films with different values of thickness and $\rho_{nuc} = \rho_{obs} = 42.8\mu\mathrm{m}^{-2}$ indented by the $\alpha = 5°$ wedge; the predictions are consistent with prior studies (*e.g.* [18, 47]). The indentation pressure variation for the size-independent elastic ($h = 50\ \mu\mathrm{m}$) film is also included to illustrate the influence of dislocation plasticity on indentation pressure. The elastic indentation pressure was divided by 5 to fit the scale, as done in [18]. The plastic calculations show the indentation size effect, *i.e.* that indentation pressure decreases with increasing contact length, hence indentation depth, before approaching a steady value provided interaction with the substrate is minimal. As in prior studies (*e.g.* [18, 35]), it is also observed that the indentation pressure for the $h = 2\ \mu\mathrm{m}$ film increases when the indentation depth $\delta > 0.1\mu\mathrm{m}$, due to the interaction between dislocation plasticity and the rigid bottom boundary. This phenomenon is more apparent in Figure 3(b), which shows nominal indentation pressure p_N versus indentation depth δ. This hardening behaviour is also observed in polycrystalline materials subjected to sub-micron indentation [46], and is strongly linked to Hall-Petch grain-size strengthening.

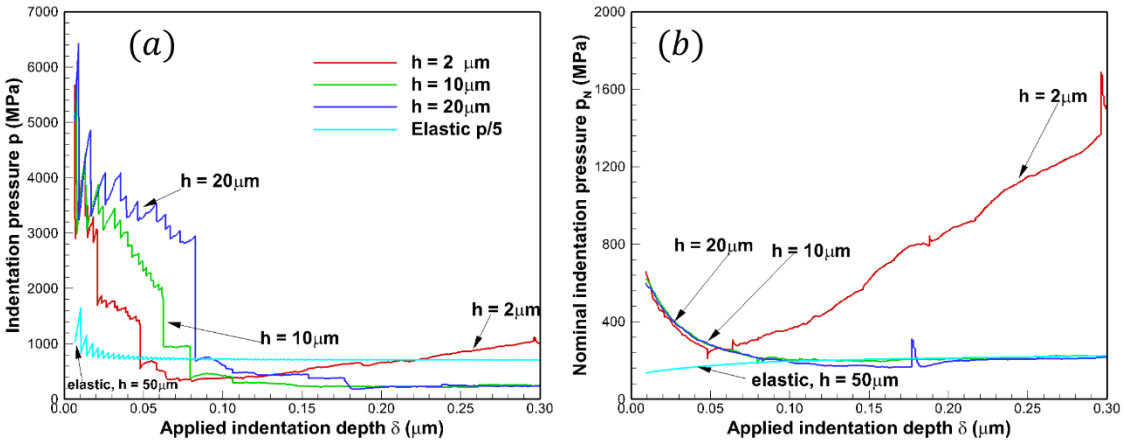

Figure 3. The (a) actual and (b) nominal indentation pressure variation of films versus applied indentation depth with the $\alpha = 5°$ wedge. Results are shown for three film thicknesses. Pressure for an elastic film ($h = 50\ \mu\mathrm{m}$) is also shown (rescaled – divided by five to fit).

The mesh size used here is more refined as $\Delta x = 5\mathrm{nm}$ within the contact under the indenter tip compared to Ref. [18] (roughly $\Delta x = 12\mathrm{nm}$), to more accurately identify the value of the contact size and thus the indentation pressure at the very beginning of the indentation process; the response at larger indentation depths is nevertheless unaffected by the additional mesh refinement. Observations in [16] of very high actual indentation pressure at low indentation depth were attributed to actual contact length remaining relatively constant

for small indentation depths, due to material sink-in, but it is also partially attributable to mesh resolution within the initial contact length.

3.2 Indentation pressure vs. indentation depth: a new physically-based formula

A shortcoming of the Nix and Gao formula is that it predicts infinite indentation pressure for infinitesimally small indentation depths, hence is not applicable for small indentation depths. In order to quantitatively predict the nominal indentation pressure, p_N, versus applied indentation depth, δ, for the entire range of indentation depths within the indentation size effect zone for thin films, the following modified form of the Nix and Gao formula is derived below:

$$p_N \equiv H = H_p + H_0\left(1 + \frac{\delta}{\bar{\delta}}\right)^{-\eta}. \tag{8}$$

In eq. (8), H_p is the depth-independent (bulk material) limit, which occurs when the applied indentation depth δ is sufficiently large compared to $\bar{\delta}$. The sum of the terms H_p and H_0 is interpreted as the initial elastic material hardness (in the $\delta = 0$ limit), and η is a material-dependent fitting parameter. The parameter $\bar{\delta}$ is a characteristic length scale parameter that is linked to the average source spacing, which will be discussed in more detail in Section 3.5.

Eq. (8) results from a modification to the model of Nix and Gao to capture the $\delta = 0$ limit and introduce a dislocation source density dependence; defect density has been shown to significantly affect the ISE in the recent experimental investigation and first-order mechanistic approach proposed by Maughan and co-workers [30]. The derivation of eq. (8) is similar to that presented in Nix and Gao [10], but with notable differences as follows. The process starts from Taylor's law [50] that relates the flow stress τ to the total dislocation density ρ:

$$\tau = \tau_Y + \alpha\mu b\rho^{1/2} \tag{9}$$

although in the derivation by [10], the intrinsic (low dislocation density) flow stress of the material, τ_Y, was not used. In eq. (9), μ is the material's shear modulus, b is the Burgers vector and α is a constant, which in Ref. [10] was assigned a value of 0.5. In Nix and Gao [10], ρ in eq. (9) is interpreted as the total dislocation density ρ_{tot}, hence in their derivation the contributions from statistically stored and geometrically necessary dislocations to hardening are assumed to combine by summation:

$$\rho = \rho_{tot} = \rho_S + \rho_G \tag{10}$$

The assumption of eq. (10) is sensible, but is not necessarily valid *a priori*, particularly given the empirical nature of the square root scaling of hardening on dislocation density in eq. (9), and the comparatively sessile nature of geometrically necessary dislocations, from which it is reasonable to expect that the contribution of GND's to hardening may be different to that of SSD's. Besides, using Taylor's scaling relationship with the dislocation density interpreted as an explicit total of SSD's and GND's in the derivation of the Nix and Gao formula leads problematically to a predicted hardness that approaches infinity as the indentation depth approaches zero. Many researchers have discussed the model shortcoming, as discussed in *e.g.* the review paper by Voyiadjis and Yaghoobi [51]. Although some attempts have been made to solve this problem, notably by Nix et al. [26, 52], by providing different methods of modifying the plastic zone volume and assigning a GND saturation cap, these and other proposed corrections are most often phenomenological in nature, and they depend upon fitting procedures.

Here we take a different interpretation of Taylor's hardening law by regarding the dislocation density as an *effective* measure of the density of dislocations that contribute to the hardening of the material, rather than as an explicit total of dislocations (notably, in Taylor's hardening law, τ_Y does not correspond to a zero dislocation density situation, hence some interpretation of ρ seems appropriate). When ρ is regarded as an *effective* dislocation density rather than an explicit total, it is also reasonable to assume that the contributions to the flow response from statistically stored, ρ_S, and geometrically necessary dislocations, ρ_G, combine in parallel, or in some other way, rather than in series:

$$\frac{1}{\rho} = \frac{1}{\rho_{eff}} = \frac{1}{\rho_S} + \frac{1}{\rho_G} \tag{11}$$

This expression, although still phenomenological in nature, allows to qualitatively capture the experimental evidence that indentation pressure decreases with the indentation depth. It follows from the above assumption that:

$$\tau = \tau_Y + \alpha\mu b\rho^{1/2} = \tau_Y + \alpha\mu b{\rho_{eff}}^{1/2} = \tau_Y + \alpha\mu b\left(\frac{1}{\rho_S} + \frac{1}{\rho_G}\right)^{-\frac{1}{2}}, \tag{12}$$

where the geometrically necessary dislocation density can be obtained from geometric arguments in terms of the indentation depth, δ, Burgers vector, b, and indenter angle, θ, as in Nix and Gao:

$$\rho_G = \frac{3}{2b\delta}tan^2\,\theta \tag{13}$$

Assuming von Mises plasticity and Tabor's factor of 3, as in Nix and Gao, the expression for the hardness is:

$$H = 3\sqrt{3}\tau = 3\sqrt{3}\tau_Y + 3\sqrt{3}\alpha\mu b\sqrt{\rho_S}\left(1 + \frac{\rho_S}{\rho_G}\right)^{-\frac{1}{2}} \tag{14}$$

Eq. (14) can also be re-written as:

$$H = H_p + H_0\left(1 + \frac{\delta}{\bar{\delta}}\right)^{-\frac{1}{2}}, \tag{15}$$

where:

$$\bar{\delta} = \frac{3\,tan^2\,\theta}{2b\rho_S} \tag{16}$$

$$H_p \equiv 3\sqrt{3}\tau_Y \tag{17}$$

$$H_0 \equiv 3\sqrt{3}\alpha\mu b\sqrt{\rho_S} \tag{18}$$

H_0 is interpreted as "*the hardness that would arise from the statistically stored dislocations alone, in the absence of any geometrically necessary dislocations*", as in [10]. As in Ref. [18], the -0.5 exponent is replaced with -η, which allowed the planar discrete dislocation plasticity predictions to accurately fit the experimental data for $\delta > 1\mu m$. Note that the length scale parameter $\bar{\delta}$ and hardness constant H_0 cannot be directly determined from eq. (16) and eq. (18), respectively, as the formulae do not account for the variation of SSD and GND densities during the deformation; furthermore, dislocations are not readily identified In DDP as either statistically stored or geometrically necessary [53], although there are methods

available that can reasonably partition the total dislocation density into SSD and GND density [54]. Instead, the determination of both parameters is detailed later, in Sections 3.3 and 3.4, respectively.

Our final formula therefore reads:

$$H = H_p + H_0\left(1 + \frac{\delta}{\bar{\delta}}\right)^{-\eta} \tag{19}$$

Again, we note that the only deviations from the derivation of Nix and Gao are in retaining τ_Y in Taylor's hardening law, and in assuming statistically stored and geometrically necessary dislocations combine *in parallel* rather than *in series*. However, these modifications mean that eq. (19) predicts a finite hardness in the $\delta \to 0$ limit and provides a direct link between the length scale $\bar{\delta}$ and the source density (see Section 3.5). In the following sections, all the parameters in eq. (19) are determined with a physically-based interpretation: in Section 3.3, the hardness constants H_p (*i.e.* the indentation depth independent continuum limit) and $H_e = H_0 + H_p$ (*i.e.* the parameter corresponding to the elastic, very small indentation depth limit) are determined, and in Sections 3.4 and 3.5 the correlation between indentation pressure variation and dislocation source density is used to link the length scale parameter $\bar{\delta}$ to the microstructure. In Section 3.6, we validate the newly proposed formula by demonstrating its ability to fit nano-indention experimental data. Note that the formula derived does not apply to situations where substrate interaction causes added hardening (see the indentation pressure response of the $h = 2\ \mu\text{m}$ film in Figure 3(b)) in addition to the indentation size effect.

3.3 Determination of hardness parameters H_p and H_0

Actual indentation pressure p_A and nominal pressure p_N curves versus applied indentation depth δ are plotted in Figure 4 (a) and (b) respectively for three films with different thicknesses. The values of nucleation source density of those films are selected as $\rho_{nuc} = \rho_{obs} = 8.28\ \mu\text{m}^{-2}$, which is an appropriate value for a low source density material. Based on Figure 4, it can be concluded that that indentation pressure evolution is not affected by film thickness provided that indentation depth does not exceeds a threshold value, beyond which the rigid boundary starts to play a role (see results for $h = 2\ \mu\text{m}$ films discussed in Section 3.1).

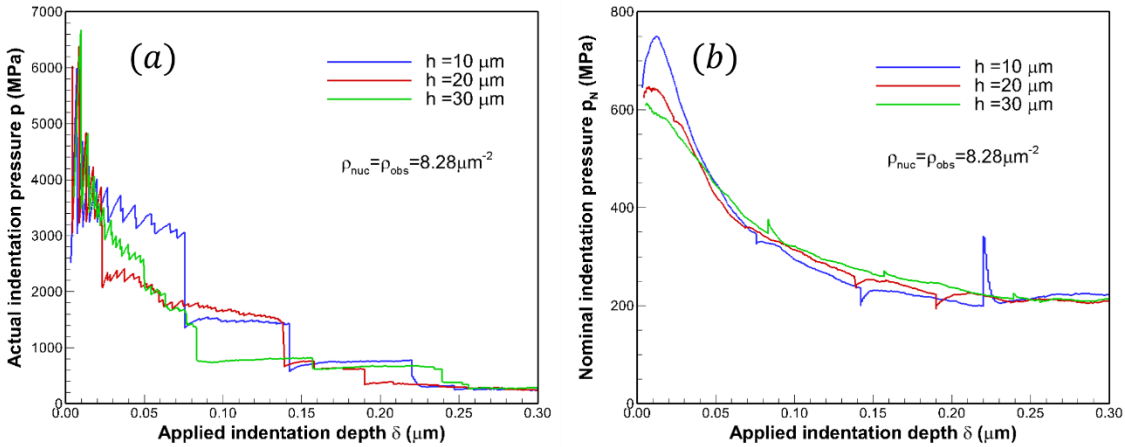

Figure 4. (a) Actual and (b) nominal indentation pressure variation of films with different values of film thickness but identical dislocation source density.

In Figure 4 (a) and (b), the $h = 10\ \mu\text{m}$ and $h = 20\ \mu\text{m}$ film curves plateau; this is the end of the indentation size effect zone where the material response is that of a continuum (*i.e.* indentation depth independent), and the plateau value is identified as the continuum hardness H_p. The value of H_p is independent of both film thickness h and dislocation source density as it represents the hardness of the bulk material in the indentation depth independent limit (as shown by the plateau value in Figure 5 (b)); the value of H_p does not account for the substrate interaction that occurs in the case of very thin films relative to the indentation depth. Thus, the value of H_p is obtained here as $H_p \cong 218\text{MPa}$ from Figure 4. It is worth noting that the value of H_p is a constant in this study as all films are comprised of a single crystal, *i.e.* there is no grain size strengthening involved; however, the value of H_p is generally observed to be dependent on the grain size of a polycrystalline film, as shown in [31], and therefore attention should be paid when quoting the correct value of hardness for polycrystalline materials characterised by different microstructures.

The hardness parameter $H_e = H_0 + H_p$ is interpreted as the elastic response at the very beginning of the indentation process. The value of H_e should not be affected by the film thickness, nor by the dislocation source density as plasticity has not yet been initiated. By extrapolation the results of Figure 4 and Figure 5 suggest there is a consistent value of the initial nominal indentation pressure, which supports this assertion; although the initial part of the indentation curve is resolved more accurately than in [16], it is not possible to resolve the finite element mesh sufficiently to accurately identify H_e from the simulations. To determine H_e, we apply Sneddon's analytical model [55], which involves nominal contact length hence is consistent with the use of eq. (19); $H_e = 1390MPa$ for aluminium subject to indentation by a $\alpha = 5°$ wedge-shaped indenter. It is anticipated that the curves shown in Figure 4(b) would extrapolate to the Sneddon value as δ goes to zero, but they are affected by the refinement of the finite element mesh for $\delta < 0.05\mu m$; extrapolating an exponential fit to the $\delta > 0.05\mu m$ data in Figure 4(b) implies a value at $\delta = 0$ of 1295MPa, which is close to the value predicted by the Sneddon formula. Although the curves in Figure 4(b) do not coincide, extrapolating individual fits to the curves to $\delta = 0$ still produces a fairly consistent value of H_e, which is roughly in-line with the Sneddon value. The details of the calculation can be found in Appendix I.

Upon obtaining the values of H_p and H_e (directly from Sneddon's formula), the value of the parameter H_0 is then calculated according to:

$$H_0 = H_e - H_p \tag{20}$$

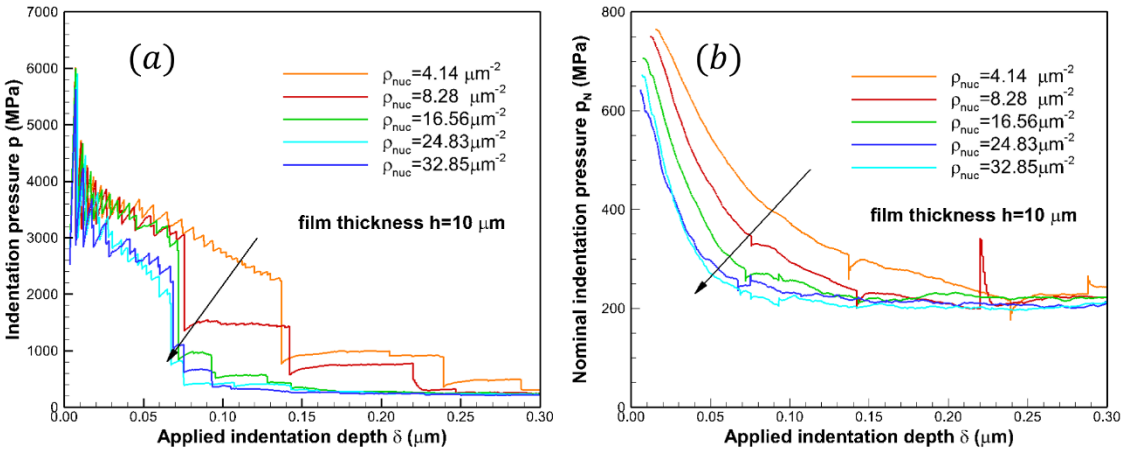

Figure 5. (a) Actual (b) nominal indentation pressure variation of films of thickness $\mathrm{h} = 10\mu\mathrm{m}$ but different nucleation source density

For the material and the indenter shape considered here, the value of H_0 is computed as $H_0 = 1180\mathrm{MPa}$.

The values of H_0 and H_p will be fixed after they have been obtained using the procedure outlined below when obtaining the best fit for indentation pressure curves using eq. (19).

3.4 The dependence of indentation pressure and length scale parameter on dislocation source density

Actual pressure p_A and nominal pressure p_N curves versus applied indentation depth δ are plotted in Figure 5 (a) and (b) respectively for a $h = 10\ \mu\mathrm{m}$ film with different dislocation structures indented by a $\alpha = 5°$ wedge-shaped indenter. Values of dislocation source density and obstacle density are varied as $\rho_{\mathrm{nuc}} = \rho_{\mathrm{obs}} = 8.28, 16.56, 24.83$ and $32.85\ \mu\mathrm{m}^{-2}$ in order to study the dependence of the indentation pressure of films on dislocation source density. As can be seen in Figure 5, both the actual and nominal indentation pressure decay faster for a larger value of the source density. This is attributed to source starvation, as observed in [16], and also in tension, bending and lattice rotation calculations [20, 56, 57]. The dislocation source density does not affect the hardness value when the indentation depth is either very small or sufficiently large.

The dependence of the indentation pressure on the source density can be quantitatively linked to the value of the parameter $\overline{\delta}$ in eq. (19). While eq. (16) approximates the dependence of $\overline{\delta}$ on statistically stored dislocation density, which is linked to the source density, the relationship can be explored directly using DDP to determine an explicit scaling relationship. A first step to understand the link between the size effect and the presence of a strain gradient is usually made by introducing geometrically necessary dislocations (GNDs) [58, 59]. However, these studies ignore other changes that occur as the dimension of the region affected by plasticity is decreased, such as the reduced availability of sources. As shown in Figure 5, the indentation pressure of a film with fewer available dislocation sources exhibits a larger value of indentation pressure at a given applied indentation depth. This source limited plasticity has also been observed in other loading scenarios, including tension [20, 21] and micro-cantilever bending [22]. We pursue an explicit formula for the dependence of $\overline{\delta}$ on the source density, similar to the relationship found between flow stress and source spacing, for example in Ref. [22].

3.5 Determination and physical interpretation of $\overline{\delta}$

Indentation calculations on $h = 10, 20, 30, 50$ and $100\mu m$ films with different source densities are performed, and the nominal indentation curves are fitted using eq. (19); details of the fitting procedure are given in Section 3.6. Three realizations of source and obstacle structures were simulated for each film thickness, as done in [60]. The fitting parameter $\overline{\delta}$ is plotted against average source spacing, $s = 1/\sqrt{\rho_{nuc}}$, (in units of 1000b) in Figure 6. The data points are averages of the three realizations for each film thickness; in each case the variance was of comparable size to the symbols used to plot the results, hence is omitted from the plot.

The value of $\overline{\delta}$ shows little or no dependence on film thickness h. However, it is evident that there is a strong relationship between $\overline{\delta}$ and the average source spacing s. Although there is a linear correlation for the majority of the simulations in the investigated range, the overall trend is sigmoidal; the plateaus for very small and large values of the average source spacing are extreme cases. In particular, the value of $\overline{\delta}$ tends to a constant positive value when the dislocation source spacing is sufficiently small, which corresponds to a saturation of dislocation sources, beyond which additional sources do not appreciably change the behaviour. In the figure we have indicated this limit as δ_p (which is around $0.25\mu m$ for the simulations and parameters investigated here).

For larger values of average source spacing the value of $\overline{\delta}$ increases in a linear fashion, which shows a similar dependence to other DDP studies [22, 47]. However, the variation of $\overline{\delta}$ levels off to a plateau value δ_e (at around $4\mu m$ in this investigation) when the average source spacing increases further. This phenomenon is due to the extreme starvation of nucleation sites leading to a more elastic behavior, which is also responsible for the perceived increased in the indentation pressure response, which preserves a relative high value at large indentation depths as shown in Figure 3a.

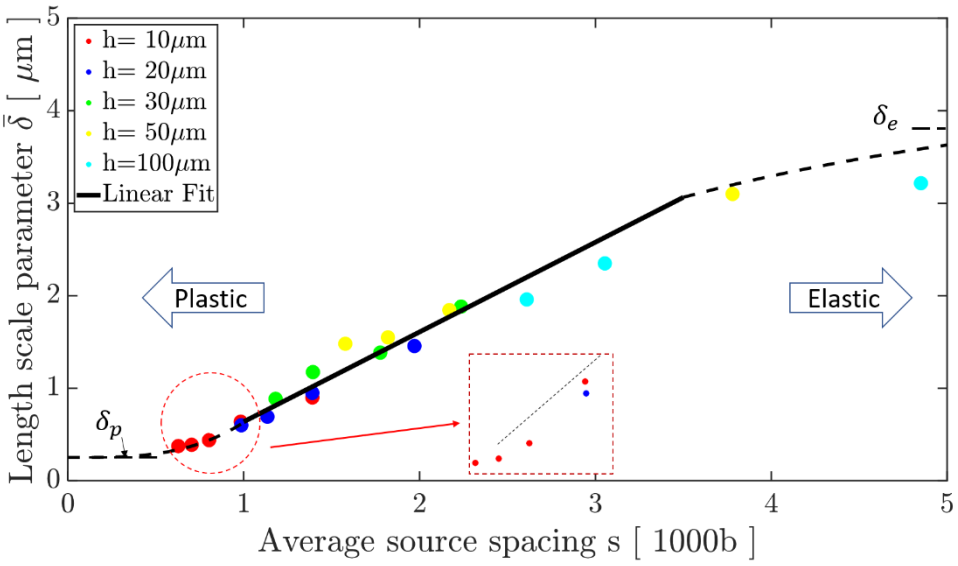

Figure 6. The linear relationship between fitting parameter $\overline{\delta}$ against average source spacing

The linear trend found for the majority of the data set can be represented by:

$$\overline{\delta} = \frac{k}{\sqrt{\rho_{nuc}}} + \overline{\delta}_0 \tag{21}$$

The best fit parameters to the data of Figure 6 using eq. (21) for different film thicknesses are tabulated in Table 2.

The slope fitting parameter k in eq. (21) reflects the sensitivity of the dependence of the length scale parameter $\overline{\delta}$ on the nucleation source density ρ_{nuc}. The constant in the linear relationship, $\overline{\delta}_0$, does not have a physical interpretation because eq. (21) does not apply in the source-saturated region when source spacing is sufficiently small (e.g. less than about 1000b). The value of k for thinner films increases with increasing film thickness; however films thicker than $h = 30\mu m$ deviate from this trend, which is attributed to the fact that the values obtained for the calculations with a large average source spacing have a much greater variance (see the R^2 value reported in Table 2 for the $50\mu m$ film) due to the extreme starvation of nucleation sites in this situation (near the δ_e limit). Hence, the fit of eq. (21) shown in Figure 5 uses only the data for the $h = 10 - 30\mu m$ films reported in Table 2. It should be noted that the linear slope calculations are also affected by the values computed for $h = 10\mu m$ when the results start to deviate from the linear trend for very small source spacing values (close to the δ_p limit). This implies that a more accurate fit could be obtained using a sigmoid function that interpolates between δ_p and δ_e and captures the linear trend between the two limits; however, this is outside of the scope of the current paper, since it depends upon accurate determination of δ_p and δ_e, which are linked to microstructural features that could be explicitly obtained by experiments. The proposed formula and the physically based length scale parameter used to correlate hardness and indentation depth provides a mechanistic understanding for the full interpretation of a thin film and coating system response under sub-micron indentation. With the benefit of direct observations and measurements [61], or otherwise indirect numerical fitting of the dislocation source density, the formula principally enables prediction of the hardness of an investigated material at a given applied indentation depth.

Table 2. Best fit parameters of the dependence of $\overline{\delta}$ on source density ρ_{nuc} using eq.(21)

$h(\mu m)$	k	$\overline{\delta}_0$	R^2
10	0.8676	-0.1462	0.9858
20	0.9154	-0.2924	0.9992
30	0.9762	-0.1532	0.9937
50	0.8923	0.2262	0.9458
100	0.8242	-0.1852	-
Overall Fit	0.9504	-0.3321	-

3.6 Fitting experimental data with the newly proposed formula

Several sets of hardness evolution data generated in nano-indentation experiments on Cu [62], Pt and Ni single crystals [30] are fitted by the proposed formula (eq.(19)) in order to verify its validity and the proposed dependence of indentation pressure on nucleation source density. For simplicity and due to lack of information available about all the materials investigated, the values of H_p and H_0 were not set *a priori* and were included in the fitting routine. However, the values found by fitting are in line with macroscopic values or those reported in the literature. In particular, the values of H_p were close to the macroscopic handbook hardness values for the corresponding metals. The experimental data and best fit curves are compared in Figure 7. As shown in the figure, the indentation size effect is successfully captured by the newly proposed formula, and the corresponding fits perform very well, with $R^2 > 0.99$.

As expected, indentation experiments were not able to detect the initial elastic hardness value H_e of specimens due to the limitations of the measurement devices. However, their values can be predicted using our fitting formula to extrapolate the corresponding curves. Other fitting parameters are also tabulated in Table 3. As mentioned above, the plastic hardness constants H_p are comparable to the macroscopic hardness values obtained in handbooks. In addition, the exponent fitting parameter η is found to within the range 0.5-0.7, which agrees with the previous predictions, such as [18, 19]. Of more significance, from the comparison between the fitting parameters of annealed and strain hardened copper specimens, the values of the parameter $\overline{\delta}$ found via the fitting verifies the strong link between the nucleation source density ρ_{nuc} and the length scale parameter: a larger dislocation source density ρ_{nuc} (strain hardened sample in the experiments) leads to a sharper decay of indentation pressure, *i.e.* a smaller value of $\overline{\delta}$ (eq.(21)). Therefore, although we cannot establish a quantitative correlation between dislocation source density and heat treatment due to the fact that the exact dislocation structures were not measured for the samples tested in the literature, the existing evidence that there are more dislocation nucleation sites in strain hardened samples [63] supports our argument and provides a good qualitative validation of the results obtained using our DDP simulations. Moreover, the decrease of the length scale fitting parameter in pure Ni specimens after being annealed [30] further confirms the dependence of indentation pressure on the dislocation source density. Our proposed formula can guide researchers to seek appropriate experimental evidence from preliminary microstructural characterisation and assessment of crystallographic defects before conducting tests; this will in turn enable to shed light on the origin of the ISE response in various materials.

These sets of experimental data are also fitted using Nix and Gao's [10] and Balint et al.'s [18] formulae, which in our notation read respectively:

$$\frac{H}{H_p} = \left(1 + \frac{\delta^*}{\delta}\right)^{1/2} \tag{22}$$

$$\frac{H}{H_p} = \left(1 + \frac{\delta^*}{\delta}\right)^{-\eta} \tag{23}$$

with δ^* now identifying the length scale parameter as introduced by Nix and Gao. Although the quality of the fitting provided by all formulae is generally good and characterised by high values of R^2, various considerations emerge from the comparisons.

The fitted continuum hardness values of the copper specimens are neither consistent between themselves (the values of size-independent hardness are $H_p = 926\text{MPa}$ using eq.(22) and $H_p = 746\text{MPa}$ using eq.(23) for annealed copper, respectively), nor agree with the empirical hardness of an annealed single crystal copper (ranging from 400-500 MPa) reported in the literature, see *e.g.* Ref. [64]. The continuum hardness value predicted using the newly proposed formula is instead consistent with this range.

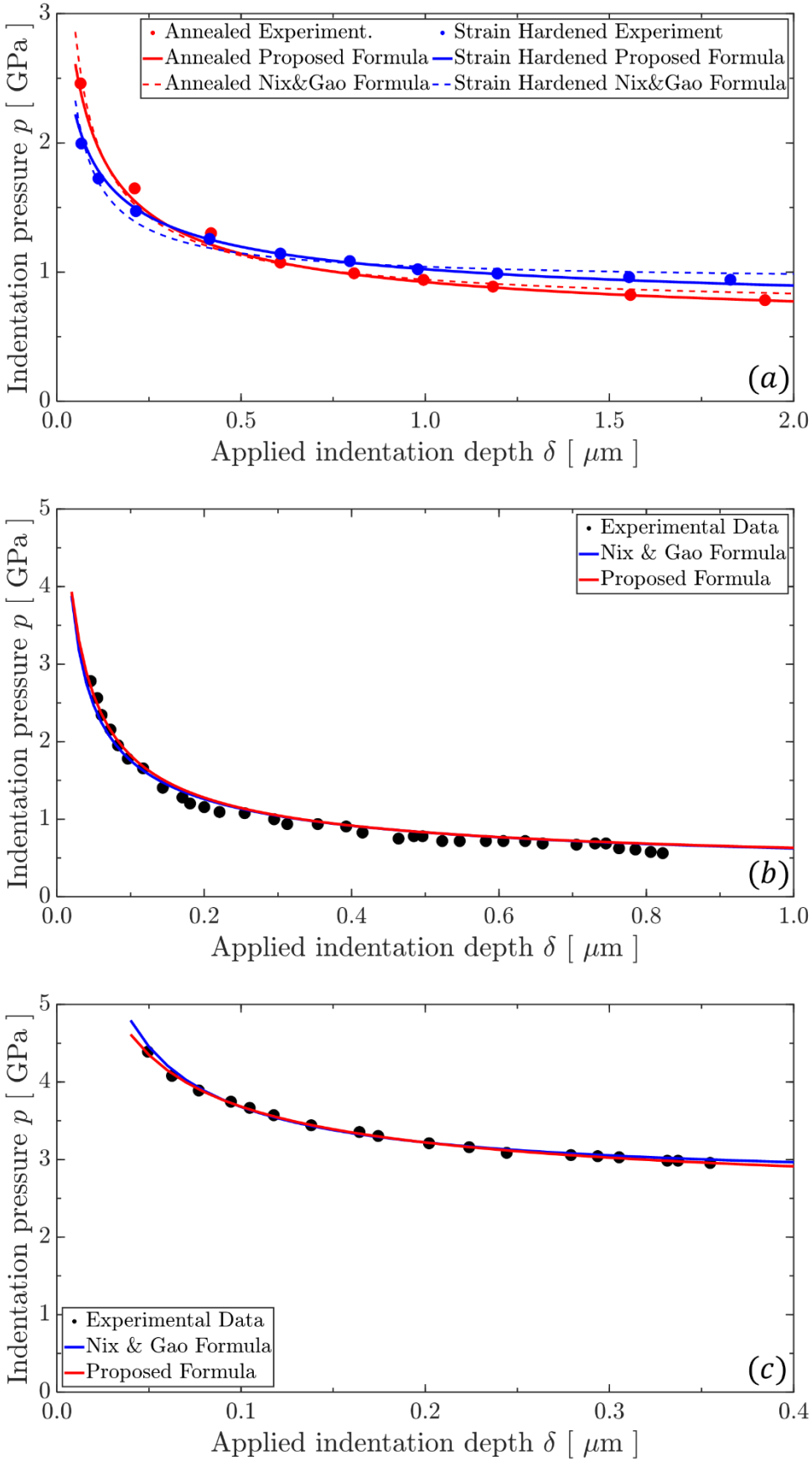

Figure 7. Hardness data (data points) and their corresponding best fit curves in the indentation size effect zone for (a) Cu single crystals, (b) Pt and (c) Ni obtained in nano-indentation experiments.

Table 3. Best fit parameters for the experimental data in Figure 7 using the new formula.

Specimen	Treatment	$H_p(MPa)$	$H_0(MPa)$	$\overline{\delta}\,(\mu m)$	η	R^2
(111) Cu	Annealed	479	3873	0.02734	0.6117	0.996
(111) Cu	Strain hardened	627	2995	0.02038	0.4941	0.991
Pt	Annealed	298	7253	0.01388	0.6927	0.992
Ni	Annealed	2330	7800	0.00641	0.6346	0.990

The fact that the continuum hardness value cannot be correctly estimated inevitably leads to a deviation from the fitting curve to the experimental data when the indentation size-independent hardness value is required as an outcome of the indentation experiments for a certain type of specimen composed of a single crystal [19], polycrystalline materials [46] or a thin coating layer (*e.g.* [65]). To illustrate this point, we have also performed the fitting by fixing the value of $H_p = 479\text{MPa}$, obtained through our analysis for annealed Cu as this is within the range of values provided in the literature, using Nix and Gao's formula (eq.(22)) and keeping δ^* as the only fitting parameter. The fitting obtained by Nix & Gao's formula with the fixed value of continuum hardness is illustrated in Figure 8, which clearly shows the potential pitfalls of the original formula if attention is not paid to its interpretation. It should be noted here that the deviation between experiments and the fitting provided by eq.(22) as proposed in Figure 8 could be improved when the length scale parameter derived in Nix and Gao's original form is corrected using a modified coefficient based on the physical interpretation of the microstructure, *e.g.* [30, 66].

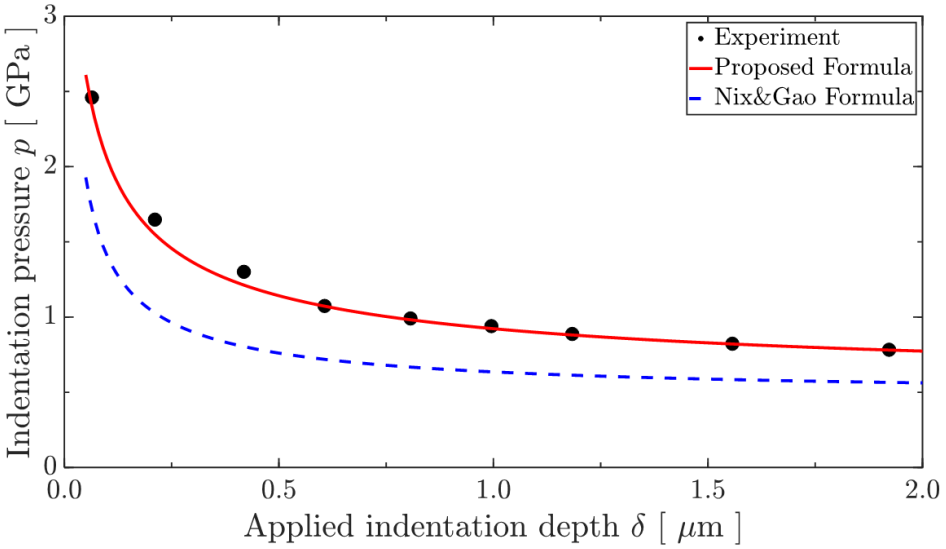

Figure 8. The deviation of Nix and Gao's formula fitting with the continuum hardness for the annealed Cu samples.

Therefore, based on the fitting results on the nano-indentation data, our new formula not only provides the indentation pressure variation with a physical interpretation of the length scale parameter within the indentation size effect zone, but also improves the previous predictions on interpreting experimental data when the applied indentation depth is relatively large compared to the film thickness.

3.7 Summary of key findings and further considerations

The DDP simulations performed in this study have allowed us to complete a thorough investigation of the size effect experienced in wedge-shaped indentation at the nano- and micro-scale. This has resulted in a multifaceted outcome. Firstly, a new formula has been proposed to fit experimental nano-indentation data, which is derived from the microstructure-based mechanisms of the indentation process, and contains fitting parameters that have been provided with a physical interpretation. They can be in principle determined through in-depth microstructural analysis and the determination of the size-independent hardness of the material and its "elastic" limit (towards zero indentation depth). Secondly, while most of the recent literature describes indentation pressure curves starting from the continuum (size-independent) hardness to the zero-indentation limit (*i.e.* from right to left along the indentation depth axis), the new formula enables capturing the entire indentation process and its transition from the initial response at nominally zero indentation depth to the size-independent limit: the hardness constants employed in the formula, H_p and H_0, not only describe the continuum hardness of a material (as in [10] and [18]), but also allow to predict the hardness value at the very beginning of an indentation process.

Another very important aspect of our investigation emerges from the evaluation of the effect that the dislocation structures (and, in particular, dislocation source density) have on the indentation process. Specimens tend to exhibit a more pronounced plastic response when there is a large number of dislocations relieving the internal stress field. Thus, indentation pressure of a specimen with more available dislocation sources decreases more apparently with the indentation depth. This prompted an investigation of the link between the length scale parameter identified in our formula and dislocation source densities, which showed a strong linear relationship between the length scale parameter and the source spacing.

We herein argue that the indentation pressure at a given applied indentation depth depends on the initial dislocation structure, more specifically, the dislocation source density of a thin film, whose value is considered as a constant during the two-dimensional indentation simulation. In fact, during an actual indentation process, the density of dislocation nucleation sites within the specimen may increase. This phenomenon has been studied using both so called 2.5D discrete dislocation dynamics plasticity (2.5D-DDP) simulations [67], which can account for this within the idealization limits of a plane strain setting, and three-dimensional discrete dislocation plasticity (3D-DDP) calculations, *e.g.* Ref. [68]. Therefore, the fact that dislocation source density can be history dependent should be considered [69]. However, for the planar problem considered here, the assumption that dislocation dipoles only nucleate from the original source population is a good first approximation, as stated in the literature [18, 20, 23]. Furthermore, evidence that the initial dislocation structure of a specimen dominates the subsequent behaviour has also been reported in simulations (*e.g.* [67, 70]) and experiments at the sub-micron scale (*e.g.* [71]). In future contributions we envisage to consider the effect that the instantaneous dislocation source density has on the indentation pressure of thin films with the aim to investigate history dependence and rate-sensitivity (*e.g.* Ref. [40]). Extending the formula to include the effect of the substrate for larger indentation depths may also lead to a physically-based unified formula to study indentation of thin films.

4 Conclusion

Plane strain analyses of single crystal films indented by a rigid wedge have been performed using discrete dislocation plasticity (DDP) employing a small-strain framework. Based on the results obtained varying film size and dislocation source density, a new indentation pressure formula has been proposed that describes the indentation pressure variation for the entire range of applied indentation depth. Fitting parameters have been provided with physical interpretation and a methodology for their determination has been provided. Furthermore, through a number of detailed computations carried out to investigate the dependence of indentation pressure of thin films upon dislocation source density, an important link between the length scale parameter identified in the new formula and the dislocation source density has been identified. This dependence, which is material dependent, is revealed as an intrinsic consequence of dislocation source saturation and starvation.

The new formula provides a very good correlation with both the simulation results considered here and relevant nano-indentation experiments. The correlation between dislocation source density and material response under indentation provides a better understanding of source limited plasticity, which has also been observed in tension and bending problems. The improved understanding of the physics governing the indentation size effect and its links to dislocation structures opens new important research avenues and important perspectives to revisit nano- and micro-indentation experiments and their interpretation.

Acknowledgments

The authors wold like to acknowledge the funding received via his Engineering and Physical Sciences Research Council (EPSRC) Established Career Fellowship awarded to Professor Dini, EP/N025954/1. All data will be made available via contacting the corresponding author or emailing tribology@imperial.ac.uk.

Appendix I

This appendix aims to show the consistency in our calculation of the value of the intrinsic hardness parameter, H_e, with Sneddon's theoretical prediction. Sneddon's analytical solution [55] of hardness of an elastic material under a rigid cone indention reads:

$$-P = \frac{2E \tan \alpha}{\pi(1-\gamma^2)}\delta^2$$

where P is the indentation reaction force, E is Young's modulus, γ is Poisson's ratio and δ is the indentation depth. The sketch below depicts schematically a certain instant of the indentation process and the key geometric parameters.

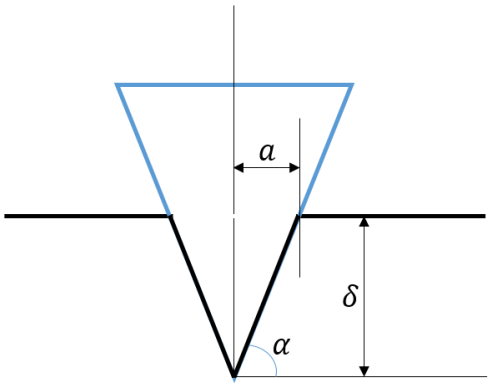

This gives the value of contact area in terms of indentation depth as:

$$A_c = \pi a^2 = \pi(\delta \tan \alpha)^2$$

Therefore, the nominal indentation pressure can be written as:

$$H_e \equiv P/A_c = \frac{2E}{\pi^2(1-\gamma^2)\tan \alpha}$$

In our simulations, the elastic constants for aluminium is given as:

$$E_{Al} = 70GPa\ \gamma = 0.33$$

And the wedge shape is described by its indentation angle, $\alpha = 5°$. Therefore, the elastic indentation pressure of aluminium pressed by this type of wedge-shaped indenter is calculated as:

$$H_{e,Al} = 1.39GPa = 1390MPa$$

Please note the initial elastic hardness is determined by the shape of the indenter and results can be equivalently determined for other indenters' shapes [72].

References

[1] D. Tabor, The hardness of metals, Clarendon Press, Oxford, 1951.
[2] K.L. Johnson, J Mech Phys Solids, 18 (1970) 115.
[3] E. Van der Giessen, A. Needleman, Model Simul Mater Sc, 3 (1995) 689-735.
[4] W.J. Poole, M.F. Ashby, N.A. Fleck, Scripta Materialia, 34 (1996) 559-564.
[5] J.G. Swadener, E.P. George, G.M. Pharr, J Mech Phys Solids, 50 (2002) 681-694.
[6] D.E. Stegall, M.A. Mamun, B. Crawford, A. Elmustafa, J Mater Res, 27 (2012) 1543-1552.
[7] K. Chen, W.J. Meng, G.B. Sinclair, Acta Mater, 60 (2012) 4879-4887.
[8] E.C. Aifantis, Internal Length Gradient (ILG) Material Mechanics Across Scales and Disciplines, in: S.P.A. Bordas, D.S. Balint (Eds.) Advances in Applied Mechanics, Elsevier, 2016, pp. 1-110.
[9] F.M. Borodich, The Hertz-Type and Adhesive Contact Problems for Depth-Sensing Indentation, in: S.P.A. Bordas (Ed.) Advances in Applied Mechanics, Elsevier, 2014, pp. 225-366.
[10] W.D. Nix, H.J. Gao, J Mech Phys Solids, 46 (1998) 411-425.
[11] A.C. Eringen, Nonlocal continuum field theories, Springer, New York, 2002.
[12] M.R. Begley, J.W. Hutchinson, J Mech Phys Solids, 46 (1998) 2049-2068.
[13] Y.G. Wei, J.W. Hutchinson, J Mech Phys Solids, 51 (2003) 2037-2056.
[14] S. Qu, Y. Huang, G.M. Pharr, K.C. Hwang, Int J Plasticity, 22 (2006) 1265-1286.
[15] Y. Guo, Y. Huang, H. Gao, Z. Zhuang, K.C. Hwang, International Journal of Solids and Structures, 38 (2001) 7447-7460.
[16] A.C. Eringen, Int J Eng Sci, 21 (1983) 741-751.
[17] J. Lou, P. Shrotriya, T. Buchheit, D. Yang, W.O. Soboyejo, J Mater Res, 18 (2003) 719-728.
[18] D.S. Balint, V.S. Deshpande, A. Needleman, E. Van der Giessen, J Mech Phys Solids, 54 (2006) 2281-2303.
[19] A. Widjaja, E. Van der Giessen, A. Needleman, Mat Sci Eng a-Struct, 400 (2005) 456-459.
[20] D.S. Balint, V.S. Deshpande, A. Needleman, E. Van der Giessen, Model Simul Mater Sc, 14 (2006) 409-422.
[21] L. Nicola, E. Van der Giessen, A. Needleman, Journal of Applied Physics, 93 (2003) 5920-5928.
[22] E. Tarleton, D.S. Balint, J. Gong, A.J. Wilkinson, Acta Mater, 88 (2015) 271-282.
[23] H.H.M. Cleveringa, E. Van der Giessen, A. Needleman, Int J Plasticity, 15 (1999) 837-868.
[24] H.G.M. Kreuzer, R. Pippan, Acta Materialia, 55 (2007) 3229-3235.
[25] K. Durst, B. Backes, O. Franke, M. Goken, Acta Materialia, 54 (2006) 2547-2555.
[26] Y. Huang, F. Zhang, K.C. Hwang, W.D. Nix, G.M. Pharr, G. Feng, J Mech Phys Solids, 54 (2006) 1668-1686.
[27] M. Rester, C. Motz, R. Pippan, J Mater Res, 24 (2011) 647-651.
[28] O. Franke, J.C. Trenkle, C.A. Schuh, J Mater Res, 25 (2010) 1225-1229.
[29] S.W. Lee, L. Meza, J.R. Greer, Appl Phys Lett, 103 (2013).
[30] M.R. Maughan, A.A. Leonard, D.D. Stauffer, D.F. Bahr, Philosophical Magazine, 97 (2017) 1902-1920.
[31] D. Balint, V. Deshpande, A. Needleman, E. Van der Giessen, Materials Science and Engineering: A, 400 (2005) 186-190.
[32] P.J. Guruprasad, A.A. Benzerga, J Mech Phys Solids, 56 (2008) 132-156.
[33] L. Nicola, A.F. Bower, K.S. Kim, A. Needleman, E. Van der Giessen, Philosophical Magazine, 88 (2008) 3713-3729.
[34] F.W. Sun, E. Van der Giessen, L. Nicola, J Appl Mech-T Asme, 82 (2015) 071009.
[35] Y. Xu, D.S. Balint, D. Dini, Model Simul Mater Sc, 24 (2016) 045007.
[36] J.R. Rice, Mech Mater, 6 (1987) 317-335.
[37] J.S. Langer, E. Bouchbinder, T. Lookman, Acta Mater, 58 (2010) 3718-3732.
[38] K.C. Le, Y. Piao, T.M. Tran, Phys Rev E, 98 (2018).

[39] A.A. Benzerga, Int J Plasticity, 24 (2008) 1128-1157.
[40] Z.B. Zheng, D.S. Balint, F.P.E. Dunne, Acta Mater, 107 (2016) 17-26.
[41] K.C. Le, T.M. Tran, J.S. Langer, Phys Rev E, 96 (2017) 013004.
[42] S.S. Shishvan, S. Mohammadi, M. Rahimian, E. Van der Giessen, Int J Solids Struct, 48 (2011) 374-387.
[43] E.C. Aifantis, Materials Science and Engineering, 81 (1986) 563-574.
[44] J. Segurado, J. LLorca, I. Romero, Model Simul Mater Sc, 15 (2007) S361-S375.
[45] V.S. Deshpande, A. Needleman, E. Van der Giessen, J Mech Phys Solids, 51 (2003) 2057-2083.
[46] A. Widjaja, E. Van der Giessen, A. Needleman, Acta Materialia, 55 (2007) 6408-6415.
[47] A. Widjaja, E. Van der Giessen, V.S. Deshpande, A. Needleman, J Mater Res, 22 (2007) 655-663.
[48] B. Gurrutxaga-Lerma, D.S. Balint, D. Dini, A.P. Sutton, J Mech Phys Solids, 84 (2015) 273-292.
[49] P.K. Agnihotri, E. Van der Giessen, Mech Mater, 90 (2015) 37-46.
[50] G. Thomas, J. Washburn, Electron microscopy and strength of crystals, Interscience New York, 1963.
[51] G.Z. Voyiadjis, M. Yaghoobi, Crystals, 7 (2017).
[52] G. Feng, W.D. Nix, Scripta Materialia, 51 (2004) 599-603.
[53] A. Needleman, Acta Mater, 48 (2000) 105-124.
[54] P.J. Guruprasad, W.J. Carter, A.A. Benzerga, Acta Mater, 56 (2008) 5477-5491.
[55] J. Harding, I. Sneddon, in: Mathematical Proceedings of the Cambridge Philosophical Society, Cambridge Univ Press, 1945, pp. 16-26.
[56] V.S. Deshpande, A. Needleman, E. Van der Giessen, J Mech Phys Solids, 53 (2005) 2661-2691.
[57] Y.H. Zhang, Y.F. Gao, L. Nicola, J Mech Phys Solids, 68 (2014) 267-279.
[58] N.A. Fleck, J.W. Hutchinson, Adv Appl Mech, 33 (1997) 295-361.
[59] N.A. Fleck, J.W. Hutchinson, J Mech Phys Solids, 41 (1993) 1825-1857.
[60] V.S. Deshpande, A. Needleman, E. van der Giessen, Scripta Materialia, 45 (2001) 1047-1053.
[61] R. Ham, Philosophical Magazine, 6 (1961) 1183-1184.
[62] K.W. McElhaney, J.J. Vlassak, W.D. Nix, J Mater Res, 13 (1998) 1300-1306.
[63] N.A. Akhmadeev, N.P. Kobelev, R.R. Mulyukov, Y.M. Soifer, R.Z. Valiev, Acta Metallurgica Et Materialia, 41 (1993) 1041-1046.
[64] G.V. Samsonov, Handbook of the physicochemical properties of the elements, Oldbourne, London, 1968.
[65] J. Chen, S.J. Bull, Vacuum, 83 (2009) 911-920.
[66] K. Durst, B. Backes, M. Göken, Scripta Mater, 52 (2005) 1093-1097.
[67] A.A. Benzerga, Journal of the Mechanics and Physics of Solids, 57 (2009) 1459-1469.
[68] H.M. Zbib, M. Rhee, J.P. Hirth, International Journal of Mechanical Sciences, 40 (1998) 113-127.
[69] J.A. El-Awady, Nat Commun, 6 (2015) 5926.
[70] H. Tang, K.W. Schwarz, H.D. Espinosa, Phys Rev Lett, 100 (2008) 185503.
[71] J.R. Greer, W.D. Nix, Appl Phys a-Mater, 80 (2005) 1625-1629.
[72] A. Widjaja, A. Needleman, E. Van der Giessen, Model Simul Mater Sc, 15 (2006) S121.